

# Properties of Short GRB Pulses in the Fourth BATSE Catalog: Implications for Structure and Evolution of the Jetted Outflows

XIU-JUAN LI,<sup>1</sup> ZHI-BIN ZHANG\*,<sup>1</sup> CHUAN-TAO ZHANG,<sup>1</sup> KAI ZHANG,<sup>1</sup> YING ZHANG,<sup>1</sup> AND XIAO-FEI DONG<sup>1</sup>

<sup>1</sup>College of Physics and Engineering, Qufu Normal University, Qufu 273165, People's Republic of China; \*Email:astrophysics0817@163.com

(Received November 30, 2019; Revised February 18, 2020; Accepted February 25, 2020)

Submitted to ApJ

## ABSTRACT

Considering the shortage of comparative studies on pulse temporal characteristics between single-peaked short gamma-ray bursts (sGRBs) and double-peaked sGRBs, we examine the pulse properties of a sample of 100 BATSE sGRBs using the BATSE Time-Tagged Event (TTE) data with a 5-ms resolution. 243 individual pulses of the single-peaked, double-peaked and triple-peaked sGRBs are fitted to get their statistical properties such as the pulse asymmetry, amplitude, peak time, and pulse width, etc. For the double-peaked sGRBs, according to the overlapping ratio between two adjacent peaks, we first define two kinds of double-peaked sGRBs as M-loose and M-tight types and find that most of the first pulses are similar to the single-peaked ones. We study the dependence of the Full Width at Half Maximum (FWHM) on the photon energy among different energy bands. Interestingly, it is found that a power-law relation with an index of -0.4 does exist between the FWHM and the photon energy for the single- and double-peaked sGRBs. More interestingly, we notice that the power-law relation with a positive index also exist for several special short bursts. In view of the three typical timescales of pulses, namely the angular spreading timescale, the dynamic timescale, and the cooling timescale, we propose that the diverse power-law indexes together with the profile evolution of GRB pulse can be used as an effective probe to diagnose the structure and evolution of the relativistically jetted outflows.

*Keywords:* gamma-ray burst: general – method: statistics

## 1. INTRODUCTION

Gamma-ray bursts (GRBs) had been studied about forty years since the first burst reported for GRB 700822 (Klebesadel et al. 1973), the physical processes and radiation mechanisms of prompt emissions still have a lot of large debates. Study of the prompt emission light-curve and the spectral evolutions can provide a good probe to learn about the nature of these problems. Many authors have investigated the pulse properties via different methods in the past decades years (e.g., Kouveliotou 1994; Quilligan et al. 1999, 2002; Norris et al. 1996, 2005, 2011; Hakkila & Preece 2011, 2014; Hakkila et al. 2015, 2018a,b). GRB temporal profiles are usually very various, irregular and complicated. There are no two bursts with the same temporal and spectral evolution found ever. Pulses as the basic radiative units of prompt gamma-ray emissions, contain the key information about the physical mechanisms and the environments in which GRBs are generated (Norris et al.

1996). Since the GRB light curves exhibit very complex structures due to the overlapping of different neighbor pulses, many attempts have been made to analyze the individual pulses instead of the mixed temporal profiles. The most efforts have been put on long GRBs with single pulses, double pulses or multi-pulses that are well distinguished and separated from each other or sGRBs including just one single pulse.

Several fitting functional forms with different numbers of parameters are used in pulse-fitting procedures for individual prompt emission and afterglows pulse (Norris et al. 1996, 2005; Ryde & Svensson 2000, 2002; Kocevski et al. 2003; Willingale et al. 2007; Liang et al. 2007). They explore many attributes of fitting-pulses including the FWHM, the pulse asymmetry, the spectral lag, the pulse amplitude, the peak time, etc., to classify long and short bursts, or to study the prompt emission mechanisms. Wider pulses tend to be more asymmetrical (Norris et al. 1996), while Kocevski et al. (2003) found that there was no significant correlation

between the asymmetry and the FWHM of pulses. The pulse amplitude is highly anti-correlated with the other pulse timing features (e.g., the rise time of pulse, the fall time of pulse, the FWHM) (Quilligan et al. 2002). For the long BATSE bursts, the pulse width is positively correlated with both the peak time and the spectral lag (Norris et al. 2005). Zhang et al. (2006) adopted a cross-correlation technique to measure the time lags of 65 single-peaked bursts and found that the lags of the vast majority of sGRBs were so small that they were negligible or non-measurable. Fenimore et al. (1995) assumed a power-law dependence of pulse width on energy. Norris et al. (1996) drew the similar conclusion with a sample of 41 bright long GRBs detected by BATSE. Other authors also studied the same power-law relation but they gave very different indexes for their samples (Peng et al. 2006; Zhang 2008; Golkhou et al. 2015; Shao et al. 2017). In addition, some literatures had investigated in details about the relation between the different timescales and temporal structures of GRBs pulses (Qin et al. 2004; Zhang et al. 2007), where three main timescales, namely angular spreading timescale, cooling timescale and dynamic timescale, had been considered to form the shapes of GRB pulses. They found that the curvature effect of the relativistic expanding spherical shell may play an important role in shaping the steep decay phase while the dynamic timescale merely contributes to the rise phase in the observed pulses when the radiative time is negligible (Lin et al. 2017). Therefore, the different timescales during the prompt  $\gamma$ -ray emission might be useful to diagnose the structure of the jetted outflows according to the pulse evolution across diverse energy channels.

The GRB spectra and light-curves vary with the expansion of fireballs and the evolution of jet structure (Beniamini & Nakar 2019; Qin 2002). von Kienlin et al. (2019) found that there was a non-thermal pulse followed by a thermal component for GRB 170817A. Goldstein et al. (2017) noted that GRB 170817A had a lower peak energy than the average value of sGRBs and a near-median fluence. Wu & MacFadyen (2018) constrained the outflow structure of GRB 170817A with a Markov Chain Monte Carlo Analysis and thought that a relativistic structured jet with an opening angle of  $\theta_0 \approx 5$  degrees, a Lorentz factor of  $\Gamma \approx 175$ , and an off-axis angle of  $\theta_{obs} = 27_{-3}^{+9}$  degrees, was largely favored. According to the multiple-wavelength observations of first gravitational-wave event GW170817/GRB 170817A, the cocoon model involving a choked or structured jet cocoon has been widely accepted as the most likely jet mechanism after the neutron-star mergers from

which sGRBs will be generally produced (Mooley et al. 2018a,b).

In this paper, we give a comprehensive study of temporal attributes for the short GRB pulses from the fourth complete BATSE catalog. Particularly, we focus on the structure analysis of the similarity or dissimilarity between single- or multiple-peaked sGRBs among different energy channels. Sample selection and data analysis are presented in Section 2. Section 3 displays our main results. Some possibly physical explanations for the pulse evolution are given in Section 4. We will end with conclusion and discussion in Section 5.

## 2. DATA AND METHOD

Our initial sample consists of 100 sGRBs selected from the fourth BATSE TTE Catalog. The photon counts of these sGRBs have been accumulated within a time bin of 5 ms into four standard energy channels, that is Channel 1 (Ch1: 25-55keV), Channel 2 (Ch2: 55-110keV), Channel 3 (Ch3: 110-320keV), and Channel 4 (Ch4:  $\geq 320$ keV). The selection criterion is that the peak count rate in any energy channels should be larger than 200 counts per second.

Based on many previous investigations, the pulses in long GRBs are typically asymmetric, i.e. fast rise and exponential decay (FRED). The pulse shapes of sGRBs are vastly hard to determine precisely because of extreme short time variability, large range of signal to noise, and finite temporal resolution, in particular for some overlapping pulses. The GRB pulse functions are however not uniquely defined. Norris et al. (1996) proposed an asymmetric exponential rise and exponential decay function.

$$f(t) = \begin{cases} A \exp[-(\frac{|t-t_{max}|}{\sigma_r})^\nu], & t > t_{max}, \\ A \exp[-(\frac{|t-t_{max}|}{\sigma_d})^\nu], & t < t_{max}, \end{cases} \quad (1)$$

where  $A$ ,  $t_{max}$ ,  $\sigma_r$ ,  $\sigma_d$ ,  $\nu$  are five parameters of a pulse,  $A$  is the normalization parameter,  $t_{max}$  is the peak time,  $\sigma_r$  and  $\sigma_d$  are the rise and decay times, and  $\nu$  measures the sharpness of the pulse. The pulse model had been easily applied to describe those spiky rather than smooth pulses of long GRBs mostly (e.g., Norris et al. 1999; Hakkila & Preece 2014; Shao et al. 2017).

From general experience of fitting purposes, Norris et al. (2005) defined another form of pulse count rate that is proportional to the inverse of the product of two exponentials, one increasing and one decreasing with time

$$\begin{aligned} f(t) &= A\lambda / [\exp(\frac{\tau_1}{t}) \exp(\frac{t}{\tau_2})] \\ &= A\lambda \exp(-\frac{\tau_1}{t} - \frac{t}{\tau_2}), t > 0, \end{aligned} \quad (2)$$

where  $\tau_1$  and  $\tau_2$  are two modulating parameters connected with the rise and the decay steepness of a given pulse,  $\lambda = \exp(2\mu)$  with  $\mu = (\tau_1/\tau_2)^{1/2}$ . At  $t = \tau_{peak} = (\tau_1\tau_2)^{1/2}$ , the intensity reaches its maximum that is normalized by  $\lambda$  to the peak intensity  $A$ . The time of pulse onset with respect to  $t=0$  has been ignored. Previously, many authors had used this model to obtain a number of pulse properties (e.g., Hakkila et al. 2008; Hakkila & Preece 2014; Hakkila et al. 2015, 2018a). Unfortunately, this model cannot be employed to physically describe the GRB pulses whose asymmetries are characterized by longer rise than decay times (Hakkila et al. 2018a). It is easy to verify that the resulting pulses always exhibit a FRED-like profile at the  $t > 0$  region even though different peak times  $\tau_{peak}$  have been assumed.

To describe the shape of long GRBs, Kocevski et al. (2003) proposed a more flexible pulse function (it was called the KRL model in Zhang & Qin (2005)) with five parameters as,

$$f(t) = f_m \left( \frac{t+t_0}{t_m+t_0} \right)^r \left[ \frac{d}{d+r} + \frac{r}{d+r} \left( \frac{t+t_0}{t_m+t_0} \right)^{(r+1)} \right]^{-\left(\frac{r+d}{r+1}\right)} + f_0(t) \quad (3)$$

in which  $f_m$  represents the maximum flux of the GRB pulse and  $t_m$  is the peak time. The quantities  $r$  and  $d$  are the two parameters describing the shape of an individual pulse.  $t_0$  denotes the offset between the start of the first pulse and the trigger time, and  $f_0(t) = at^2 + bt + c$  represents a background at the observation time  $t$ . By contrast, the KRL pulse model with six free parameters for constant background can reproduce any types of profiles (Kocevski et al. 2003; Zhang & Qin 2005; Zhang et al. 2006, 2007; Li et al. 2020) and is thus more flexible and universal if only the same real instead of incident data from telescopes have been utilized.

Of course, which pulse fitting model is taken is largely irrelevant, given the obliging nature of GRB time profiles and the fact that the “detected” (processed through the detector response) rather “incident” flux is being modeled. Considering the above differences between three models and the variety of sGRB pulses, we empirically choose the KRL model for our current investigations. Due to the disturbance of white noises and backgrounds, the GRB pulses often become brighter with random fluctuations. So we adopt an adjacent-averaging method to smooth the original light curves and give further background subtraction before fitting. Note that three points as the smoothing window have been chosen to extract the complete information of GRB pulses.

For this study, we firstly estimate the background level ( $1\sigma$ ) and extract the effective pulse signals at a confidence level of  $S/N > 3\sigma$ . Relatively, the single-peaked sGRBs called as SPs in Figure 1 (a) are very easily distinguished. In the case of multiple-peaked sGRBs, we have used the least Chi-Square criterion to identify how many components within one burst as done by some previous authors, (e.g., Norris et al. 1996; Kocevski et al. 2003; von Kienlin et al. 2019). Once a sGRB is distinguished to have double peaks (DPs) with a M-like shape, we then divide them into the M-tight types (Mt-DPs) in Figure 1 (b) and the M-loose ones (Ml-DPs) shown in Figure 1 (c), depending on whether the intensity percentage of trough of peaks is higher than 10% or not (see also Norris et al. 2005; von Kienlin et al. 2019). After excluding some sGRBs with very complex structures, caused by the heavy overlapping between adjacent pulses, usually having more than three components, the refined sample with well-fitting consists of 81 sGRBs including 57 SPs (57%), 22 DPs (22%), and 2 triple-peaked GRBs (TPs, 2%) (see Figure 1 (d)). Totally, 243 individual pulses have been carefully analyzed in details.

### 3. RESULTS

#### 3.1. Pulse Properties

We study the asymmetry, width, amplitude and energy dependence of sGRB pulses. For the SPs, pulses in Ch2 and Ch3 are compared to check the evolution of pulse shape with the  $\gamma$ -ray energy. For two types of the DPs, the numbers of them are relatively limited so that we add together the channels 2 and 3 in order to increase statistical reliability.

##### 3.1.1. Asymmetry and Width

As usual, the asymmetry of a pulse is defined to be a ratio of the rise time  $t_r$  of full width at half maximum (FWHM) to the decay time  $t_d$  (e.g., McBreen et al. 2001; Zhang & Xie 2007). It is noticeable that with the asymmetry is difficult enough to determine in lGRBs (Kocevski et al. 2003), and can be much more so in sGRBs. The systematic errors of pulse measurements are estimated with error propagation according to Zhang et al. (2006). Figure 2 shows that the  $t_r$  and the  $t_d$  are good in agreement with a power-law relation of  $t_r \sim t_d^\beta$  for the SPs and the DPs, except the Ml-DPs. The power-law indexes are listed in Table 1. Interestingly, these results for sGRBs are much similar to those of long GRBs (Norris et al. 1996). For the Ml-DPs, the power law correlation is less tight than that of the Mt-DPs, especially for the second pulses whose  $t_r \sim t_d^\beta$  seems to be inexistent. It needs to emphasize that the

power law correlation between the  $t_r$  and the  $t_d$  of the first pulses in the DPs is very consistent with that of the SPs. In addition, the power law correlations in both the first and the second pulses of the Mt-DPs are relatively tighter than those of the MI-DPs. It is also found that the measured parameters of DPs have relatively large statistical uncertainties than those of the SPs, hinting a trend of more pulse numbers more difficult to measure. Meanwhile, we find that the critical parameters  $r$  and  $d$  of sGRB pulses obviously hold larger scatters in contrast with IGRB pulses.

From Figure 3 and Table 2, we obtain that the asymmetries of all three kinds of sGRBs range from 0.04 to 1.48 and have a mean (median) value of 0.79 (0.81). This result is slightly larger than the value of 0.65 measured for a sample of 100 bright BATSE sGRBs by [McBreen et al. \(2001\)](#), however, it is quite close to the value of 0.81 given for the single-peaked sGRBs ([Zhang & Xie 2007](#)). Especially, we find the mean asymmetry of the SPs is very similar with that of the 1st pulses of the two kinds of DPs. It is worthy to point that the averaged asymmetries of the SPs and the 2nd pulses in the DPs are largely different, which implies that the SPs and the 1st pulses in DPs could share the same origin. For the two TPs in trigger #06715 and #07102, their pulse asymmetries will evolve with time, which hints that the second or third pulse could be produced from different emitting regions.

Figure 4 shows the distributions of  $t_r/t_d$  for the SPs pulses and the 1st pulses of the two subclasses of the DPs. A K-S test gives the probabilities of  $P_{SP2,SP3} \sim 0.37$  with  $D_1 \sim 0.17$ ,  $P_{SP2,Mt1} \sim 0.37$  with  $D_2 \sim 0.20$ ,  $P_{SP2,Mt1} \sim 0.84$  with  $D_3 \sim 0.20$ , indicating that the four distributions are drawn from the same parent distribution. Figure 5 shows that the pulse width and the asymmetry are not correlated for the sGRB pulses. This phenomenon is similar to that found by [Kocevski et al. \(2003\)](#), while it is inconsistent with [Norris et al. \(1996\)](#) for long bursts. Surprisingly, both pulses in the MI-type sGRBs, unlike those in the Mt-DPs and the SPs, exhibit a coincident weak anti-correlation between the FWHM and the asymmetry, that is more wide more asymmetric, which may hint a distinct geometrical or physical mechanism for these kinds of bursts. Note that the dependence of the FWHM on the asymmetry in the second pulse is relatively weaker than that in the first pulse of the MI-DPs.

Moreover, we study the relation of the peak time ( $t_m$ ) with the asymmetry appears to also have no significant law in Figure 6, from which we notice that the  $t_m$  and the  $t_r/t_d$  are independent for the SPs, the Mt-DPs and the 1st pulses in the MI-DPs. It is surprisingly found

the  $t_m$  is anti-correlated with  $t_r/t_d$  for the 2nd pulse in the MI-DPs, as shown in Figure 5 Panel (c) in Figures. 5– 6 seems to show that the 2nd pulses in the MI-DPs have a diverse formation mechanism from other types of pulses.

Figure 7 indicates that the  $t_m$  and the FWHM are positively correlated with a form as  $t_m \sim \mu FWHM$ , which is consistent with the previous result of IGRBs of BATSE ([Norris et al. 2005](#)). The fitting results are listed in Table 3. It proves again that the characteristics of the 1st pulse of two subclasses of the DPs and the SPs are very similar and hence they may share the same origin from the central engine.

### 3.1.2. Pulse Amplitude

The pulse amplitude ( $f_m$ ) reflects the released energy amount of the interactions between internal shocks. Figure 8 demonstrates that there is no obvious correlations between the  $f_m$  and the  $t_r/t_d$  for either the SPs or the DPs. Figure 9 indicates that the  $f_m$  of the SPs is lognormally distributed with a mean value of  $f_{m,SP} = 2884.03^{+206.27}_{-192.50}$  counts/s. Figure 10 gives the mean values of the  $f_m$  to be  $f_{m,Mt1} = 2344.23^{+54.60}_{-53.36}$  counts/s for the 1st pulses and  $f_{m,Mt2} = 1905.46^{+44.80}_{-85.76}$  counts/s for the 2nd pulses of the Mt-DPs. For the MI-DPs, the mean values of the  $f_m$  are  $f_{m,Mt1} = 1737.80^{+40.48}_{-39.56}$  counts/s in the 1st pulses and  $f_{m,Mt2} = 2511.89^{+118.38}_{-113.06}$  counts/s in the 2nd pulses. The results indicate that the released energy amount in the 1st pulses of the Mt-DPs is usually larger than that in the 2nd pulses while it is opposite for the MI-DPs, which demonstrates that these two kinds of DPs might originate from different physical processes in essence. Figure 11 shows that the  $f_m$  and the FWHM are anti-correlated with a power-law form of  $f_m \sim FWHM^\nu$  that is consistent with the previous conclusion drawn for long GRBs ([Quilligan et al. 2002](#)). The power-law indexes are listed in Table 4. For the MI-DPs, the power law index of the 1st pulse is larger than that of the 2nd one. On the contrary, for the Mt-DPs, the index of the 1st pulses is smaller than that of the 2nd one. The opposite result suggests again that the two M-type DPs might be produced by different kinds of mechanisms originally.

### 3.2. Relation of width with Energy

To test whether the power law relation,  $FWHM \propto E^\alpha$ , of the pulse width with the photon energy hold for the sGRBs, we select those qualified sGRBs detected in three channels at least to ensure the relation between the FWHM and the photon energy can be successfully constructed. Since the photon fluxes in Ch1 and Ch4 are



usually too weak to be detected significantly, we sometimes need to combine the two channels with Ch2 and Ch3, respectively. Considering the errors of  $f_m$ ,  $t_m$ ,  $r$  and  $d$ , the error of the FWHM is estimated with error propagation according to our previous work (Zhang et al. 2006). In general, we adopt the averaged photon energy in the first three channels and 500 keV to be the estimated energy of photons in the fourth channel. Table 5 lists our detailed fitting results.

Figure 12 – 13 display the fitted 17 SPs with negative power-law indexes. The mean value of the negative indexes is  $\alpha \simeq -0.32 \pm 0.03$  that is very close to the results gotten by Fenimore et al. (1995) and Norris et al. (1996) for the pulses of long bursts. On the other hand, we surprisingly find that three SP sGRBs have positive power-law indexes whose mean value is about  $\alpha \simeq 0.29 \pm 0.09$  as shown in Figure 14. In addition, we select four DPs to compare with the above results of the SPs in Figure 15 (a) and (b), where it can be seen that the power law indexes in the first and the second pulses of the Mt-DPs, unlike the those of the MI-DPs, are inverse and inconsistent. The mean values of these negative and positive power-law indexes are  $-0.49 \pm 0.14$  and  $0.19 \pm 0.05$ , respectively for the 1st and the 2nd pulses in the Mt-DPs. For the MI-DPs, both two pulses of # 02115 have a mean index value of  $\alpha \simeq -0.42 \pm 0.03$  that is well consistent with that of long GRBs. Peng et al. (2006) studied two samples of long BATSE bursts taken from Kocevski et al. (2003) and Norris et al. (1999) and found that five bursts behave a positive index power-law correlation between the FWHM and the photon energy. They pointed out that the formation mechanism of the positive correlation was unknown. Very excitingly, we claim that the positive power law correlations not only exist in long GRBs, but also appear in some of the SPs and the DPs.

Interestingly, Norris et al. (2011) studied the heterogeneity of *Swift*/BAT sGRBs and found that pulse peak intensity and pulse interval or width are strongly (weakly) anti-correlated with each other for sGRBs without (with) extended emission (EE) components or for some lGRBs (Hakkila et al. 2008; Hakkila & Preece 2011), which means the pulse width and the interval are proportionally related for both short and long bursts, at least parts of them. Since the pulse intensity is tightly relevant to the total  $\gamma$ -ray energy, the negative correlation of  $FWHM \propto E^\alpha$  is naturally expected. Zhang et al. (2007) proposed that short and long GRBs respectively occurred at smaller and larger radii from their central regions (Zhang et al. 2007). If the pulse timescale is mainly contributed by the accretion process to an incipient black hole (Norris et al. 2011), the inconformity

of pulse emission strength (or energy), width or interval between two kinds of bursts can resulted from their different emitting radii.

### 3.3. Temporal Evolution

Owing to the joint effects of radiation processes, geometries and dynamics of outflows, the observed temporal profiles usually evolve with both the time and the frequency in the observer frame. Figures 16 and 17 exhibit two typical examples with temporal evolutions from lower to higher energy channels. We can see from Figure 16 that # 02126, as one of three SPs with positive power-law index in the relation of  $FWHM \propto E^\alpha$ , obviously changes from the asymmetrical shape in lower energy band to the symmetrical one in the higher energy band. The values of  $t_r/t_d$  are 0.12, 0.31, 0.49 and 0.88 in channels 1, 2, 3 and 4, respectively. Hereafter, we call this evolution sequence as “MODE I”. On the contrary, # 00432 as another SP sGRB has a common negative power-law index,  $\alpha$ , and evolves in shape in an opposite way roughly, which is defined to be “MODE II”. The values of  $t_r/t_d$  of # 00432 from the lower to the higher channel are 1.24, 0.64, 0.56, and 0.66 corresponding to channels 1-4 individually. Furthermore, we analyze the evolution behavior of the first pulses of the Mt-DPs and find that the temporal profiles of # 02217 and # 07901 with a negative index  $\alpha$  are much similar to the SPs becoming more and more symmetrical. However, the 1st pulse of # 03113 with a positive index  $\alpha$  is different from # 02126 and # 00432.

## 4. IMPLICATIONS

In this section, we will focus on how to explain the regular evolution of two kinds of GRB pulses across different energy channels. The varieties of GRB pulses can naturally reflect the activities of central engine, together with the geometry of the jetted outflows. As mentioned in Zhang et al. (2007), the temporal profiles of GRB pulses are usually determined by three main timescales, namely the angular spreading timescale,  $T_{ang} = R_c/(2\Gamma^2 c)$ , the dynamic timescale,  $T_{dyn} = \Delta'/(2\Gamma v'_{sh})$  and the cooling timescale,  $T_{syn} = t'_\gamma/\Gamma$ , where  $R_c$  is the radius of emission region,  $\Gamma$  is the bulk lorentz factor of the outflow,  $c$  is the speed of light in vacuum,  $\Delta'$  is the thickness of shell and  $v'_{sh}$  is the velocity of shock relative to the pre-shocked flow, and  $t'_\gamma$  is the radiative timescale in co-moving frame of the shell. In different phases after a burst, the above three timescales will change with time or radius. For instance, the cooling timescale  $T_{syn}$  possibly becomes longer than the other two timescales at a larger radius so that the resulting pulse profiles could behave a

quasi-FRED but more symmetric feature with smoother peaks (Zhang et al. 2007; Spada et al. 2000). In other words, the pulse shapes would be dominated by parts of these timescales in a certain emitting region. For simplicity, we assume that one GRB pulse has been generated from internal collision shocks within a two-component jet as illustrated in Figure 18, where  $\gamma_j$  and  $\gamma_c$  are lorentz factors of the inner jet and the exterior cocoon, respectively. Besides, the  $\gamma_j$  is always far larger than the  $\gamma_c$  in any cases. We also caution that the outward cocoon around the jet may have a sub-relativistic velocity, instead of the non-relativistic one inferred for GRB 170817A (Mooley et al. 2018a,b; Ghirlanda et al. 2019).

The temporal evolution “MODE I” can be easily explained if the Figure 18 is considered on-axis as follows. At early stage 1, the cocoon envelope ahead of the jet surface will be accelerated by the inner jet at larger angle range due to the viscosity of the outflows. The earlier soft  $\gamma$ -rays are mainly produced from the sub-relativistic cocoon that is heavily suffered from the curvature effect. This will result in the FRED-like pulses as we have seen in lower energy channels, for instance the upper left and right panels of Figure 16. Since the inner jet moves outwards far faster than the outer cocoon, the jet will pass through the cocoon and start to contribute  $\gamma$ -rays dominantly to the GRB pulse in higher energy channels from the stage 2 to 3. At this moment, the temporal profiles dominated by higher energy photons are primarily resulted from the dynamic and synchrotron timescales in that the newborn jet is much narrower than the forgoing cocoon, which leads to the observed pulses become more and more symmetrical. Of course, if the jet-cocoon system is seen at a off-axis angle of  $\theta_v$ , the spreading angular timescale will play more important role on shaping the pulses.

Regarding the “MODE II”, we intend to interpret it by taking into account an isolate jet without a cocoon accompanied. In fact, for most of sGRBs, the surrounding cocoons are not always necessary on modeling the potential progenitors. Here, we assume that the cocoon in Figure 18 does not exist from the beginning and prompt  $\gamma$ -rays are only emitted from the relativistic jet. In early phase after the jet was launched, its initial opening angle is too narrow to contribute more  $\gamma$ -rays influenced by the curvature effect significantly. Thus the early pulses in lower energy channels would be mainly determined by the dynamic and synchrotron timescales and behave more symmetrical. With the processes of the acceleration of the jet and its interaction with circum-burst medium, the effect of sideways expanding (Rhoads 1999; Sari 1999) on the spreading an-

gular timescales should be more significant than before. Naturally, the observed pulses in this situation will have the FRED-like shapes as displayed in Figure 17. In addition, the trend of the FRED will be strengthened if the jet is viewed from a larger off-axis angle.

## 5. CONCLUSIONS AND DISCUSSIONS

In this paper, we have systematically studied the statistical properties of short BATSE GRBs and achieve the following conclusions.

- There is a consistent power-law correlation between the rising time  $t_r$  and the decay time  $t_d$  for the SPs and the first/second pulse of the DPs, except the second pulse of the MI-DPs, which may suggest that two types of DPs might be originated from different physical processes. Also, we verify that the distributions of the asymmetry in the SPs and the first pulses of the DPs are drawn from the same parent distribution. The mean value of the asymmetry  $t_r/t_d$  of the SPs is consistent with some previous results gotten by Zhang & Xie (2007), showing again the pulses in sGRBs are more symmetrical than long GRB pulses.
- On the whole, there are no obvious relationships of the asymmetry with pulse width, the peak time  $t_m$  and the amplitude  $f_m$ , respectively, found for the SPs and the DPs of the sGRBs, except the second pulses in the MI-DPs that behave weak dependence of the  $t_r/t_d$  on the FWHM and the  $t_m$ . This may hint that the MI-DP indeed has a unique origin. The result of the asymmetry uncorrelated with the width is coincident with the previous finding for long GRBs by Kocevski et al. (2003).
- We have studied the  $f_m$  distributions contrastively and concluded that the averaged magnitude of the SPs is clearly higher than those of the first/second pulses in the DPs. It is surprisingly found that the released energy amount in the 1st pulses of the Mt-DPs is larger than that in the 2nd pulses, while it is opposite for the MI-DPs, which may demonstrate again that these two kinds of DPs are largely different in physical processes.
- To compare the power-law relation,  $FWHM \propto E^\alpha$ , of the photon energy with the pulse width of the sGRBs with that discovered for long GRBs previously, we chose both the SPs and the DPs as our research targets. Interestingly, not only the traditionally negative but also the peculiarly positive energy correlations are found to coexist in either the SPs or the DPs. We noticed that the

negatively mean index of  $\langle \alpha \rangle \sim -0.3$  for the SPs is very close to some previous results of long GRBs (e.g. Fenimore et al. 1995; Norris et al. 1996). For the DPs, it is hard to obtain the reliable power law index  $\alpha$  statistically due to the currently limited samples.

- Finally, we studied the evolution of different kinds of pulses in sGRBs across diverse energy channels and found two regular evolving modes, namely the “MODE I” and the “MODE II”, for the first time. Importantly, we speculated that the two evolving modes of pulses could universally appear in most of GRBs. More importantly, we proposed that the regular types of “MODE I” and the “MODE II” can be used as a probe to explore the structures, evolutions and orientations, etc, of the relativistic outflows, especially in cases of the off-axis and lateral expansion. However, the current samples with the two precise modes are relatively small in the BATSE catalog. It is vastly encouraged to search for more samples with the standard modes from other GRB catalogs, such as Fermi/GBM, HXMT/HE, *Swift*/BAT.

Some similarities of long and short GRBs in respect of the observational properties of prompt gamma-rays had been shown in (Ghirlanda et al. 2015). Regarding the softer X-rays, interestingly, it had been pointed out by Margutti et al. (2011) that the early X-ray flares of short GRBs behaved as those of long GRBs. Recently, Hakkila et al. (Hakkila & Preece 2014; Hakkila et al. 2015, 2018a) examined the residuals in their fits to long, intermediate and short GRB pulses and found three separate wave-like peak structures in the residuals for each pulse. Then they suggested that the complex GRB profiles may be composed of fewer pulses than the apparent number of peaks. This might help us to understand the diversity of multiple pulses in some bursts, other than the aspect of physical mechanisms.

The internal energy dissipation processes of GRBs include the precursors emissions caused by shock breakout or photosphere emissions (Lyutikov & Usov 2000; Campana et al. 2006), prompt  $\gamma$ -ray emissions (the main emission), EE as well as late X-ray flares (Hu et al. 2014). The precursors and the EE had been investigated by many previous authors (e.g., Lyutikov & Usov 2000; Campana et al. 2006; Zhang et al. 2018; Lien et al. 2016; Lan et al. 2018; Zhong et al. 2019). Similarly, the precursors and the EE components might be physically related with the main radiations of  $\gamma$ -rays and are expected to disclose more progenitor information for the sGRBs (Li et al. 2020, in preparation). For brighter sGRBs,

the EE component is sometimes detectable above the background (Norris & Bonnell 2006). One SP (#07427) and one DP (#00575) in our sample are two EE bursts from Hakkila et al. (2018a) and Bostanci et al. (2013). However, we cannot fit the EE episodes with the pulse model because of their low signal-to-noise as in Hakkila et al. (2018a). In practice, the EE components are more readily perceived in *Swift*/BAT mask-tagged data for sGRBs, we have examined in details their temporal and spectral properties and possible connections with main peak episodes (Li et al. (2020), in preparation).

Very recently, an interesting work on multiple pulses of Fermi/GBM GRBs had been done by Li (2019) to search for an evidence of the transition from fireball to Poynting-flux-dominated outflow in the GRB160602B-like sample. As a result, he found 9 out of 41 GBM bursts to be coincident with the case. Note that multiple pulses in each of the 41 bursts can be clearly separated. Actually, the prompt  $\gamma$ -rays emitted from smaller to larger radii should be naturally composed of different radiative components. The reason is that the early and late dominant radiation mechanisms are generally the thermal emissions from the photospheres and the non-thermal (synchrotron) emissions from the Poynting fluxes. According to Li (2019), the differences between the MI-DPs and other sGRBs with the SPs and the Mt-DPs can be easily explained if the MI-DPs are assumed to occur the transition process from fireball to Poynting-flux-dominated outflow. Based on the above discussions, we believe that the observed profiles of GRB pulses are affected by not only the geometry, the dynamics and the radiative cooling of outflows, but also the detailed radiation mechanisms. Certainly, the distinct radiation mechanisms will lead to different radiative cooling processes. Therefore, it is very urgent to clarify the fraction of the SPs belonging to the MODEs I and II, and distinguish how the diverse radiation mechanisms affect on the shape of all kinds of pulses in details in the future.

#### Acknowledgements

We are very grateful to the anonymous referee for his/her comments, which helped us to improve the manuscript greatly. This work made use of the data supplied by the High Energy Astrophysics Science Archive Research Center (HEASARC) for the on-line CGRO/BATSE catalog. It was partly supported by the Natural Science Foundations (ZR2018MA030, XKJJC201901).

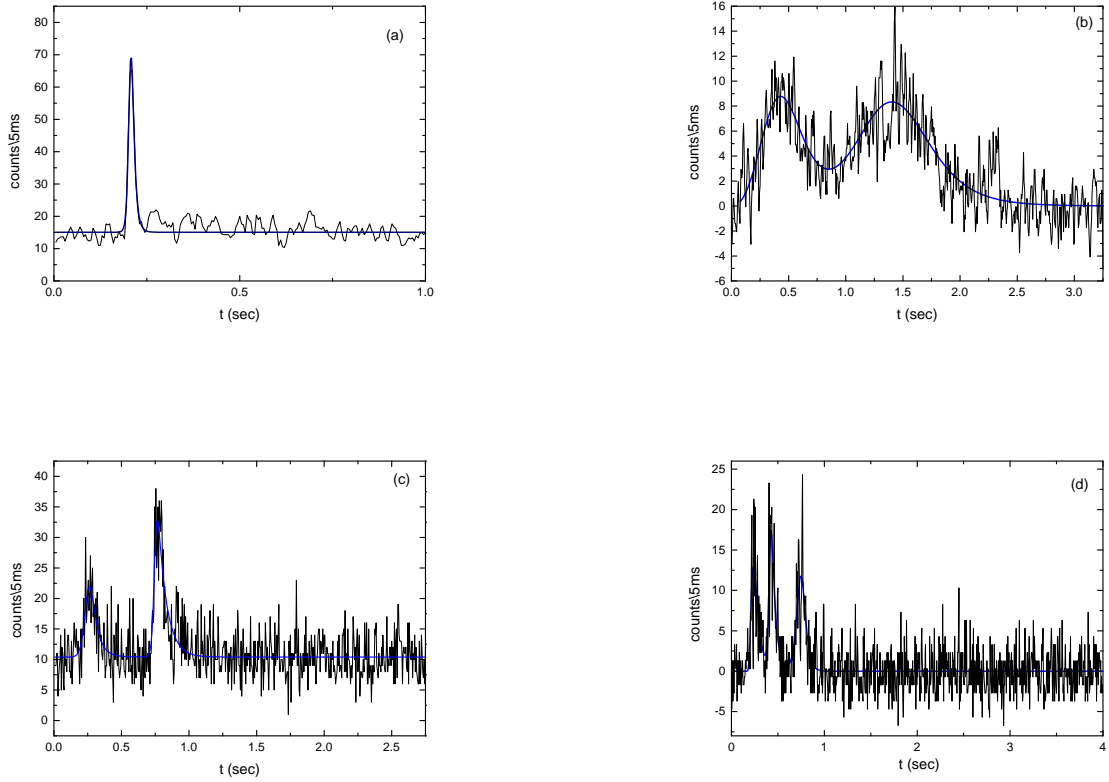


**Figure 1.** Several typical light curves of the sGRBs. (a) SPs with trigger number # 0512 (Ch2). (b) Mt-DPs with trigger number # 03113 (Ch2). (c) Ml-DPs with trigger number # 02115 (Ch3). (d) TPs with trigger number # 07102 (Ch3).



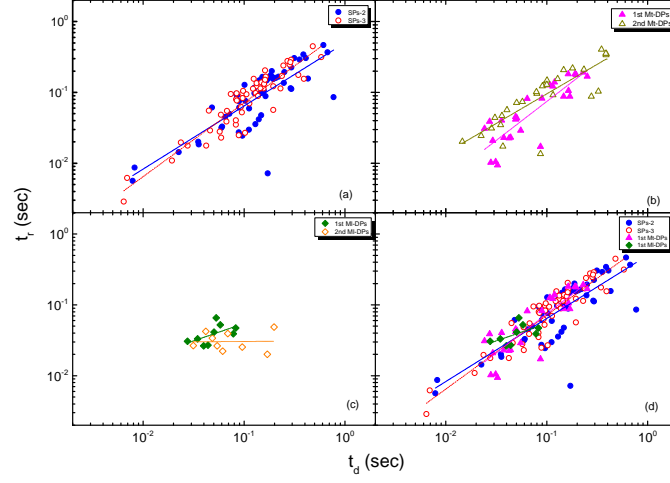


**Figure 2.** Correlations between the  $t_r$  and the  $t_d$  for different kinds of sGRB pulses. (a) The filled and the open circles represent the SPs in Ch2 and Ch3, respectively. (b) The filled and the open triangles represent the 1st and the 2nd pulses of the Mt-DPs. (c) The filled and the open diamonds represent the 1st and the 2nd pulses of the MI-DPs. (d) Comparisons between the SPs and the 1st pulses of both the MI-DPs and the Mt-DPs. All the lines stand for the best fits to the data.

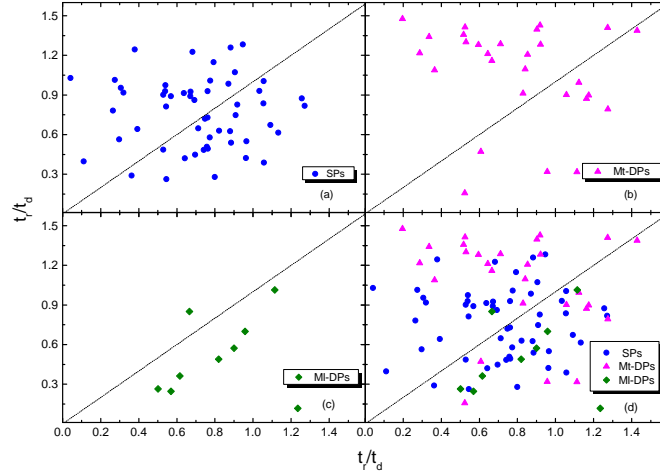


**Figure 3.** Comparisons of the  $t_r/t_d$  for all three kinds of sGRB pulses. (a) asymmetries of the SPs pulses in Ch2 versus Ch3. (b) asymmetries of the 1st versus the 2nd pulses in the Mt-DPs. (c) asymmetries of the 1st versus the 2nd pulses in the MI-DPs. (d) comparison of the asymmetries between the SPs, the MI-DPs and the Mt-DPs.

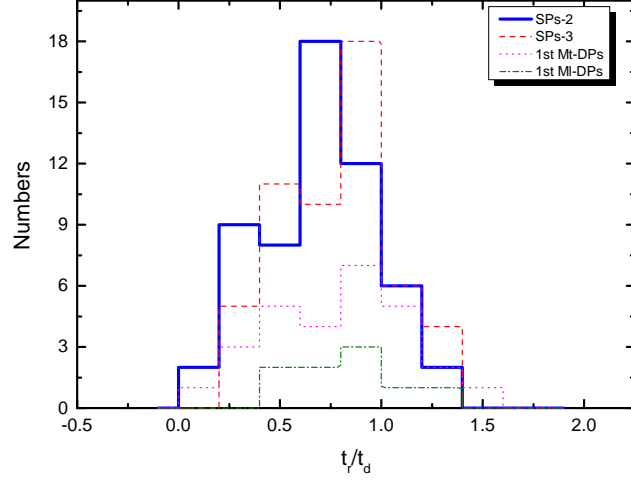


**Figure 4.** Distributions of the  $t_r/t_d$  of all three kinds of sGRB pulses: the SPs pulses in Ch2 (solid line) and Ch3 (dash line), the 1st pulses of the Mt-DPs (dot line) and the 1st pulses of the MI-DPs (dash dot line)

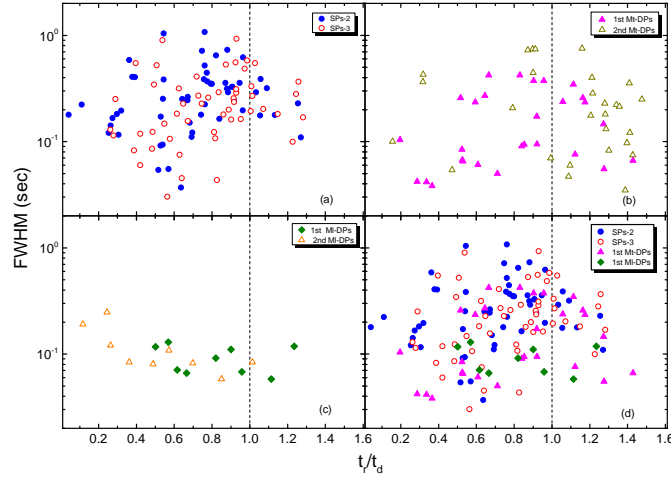


**Figure 5.** Correlations between the FWHM and the  $t_r/t_d$  of all three kinds of sGRB pulses. The symbols are the same as Figure 2.

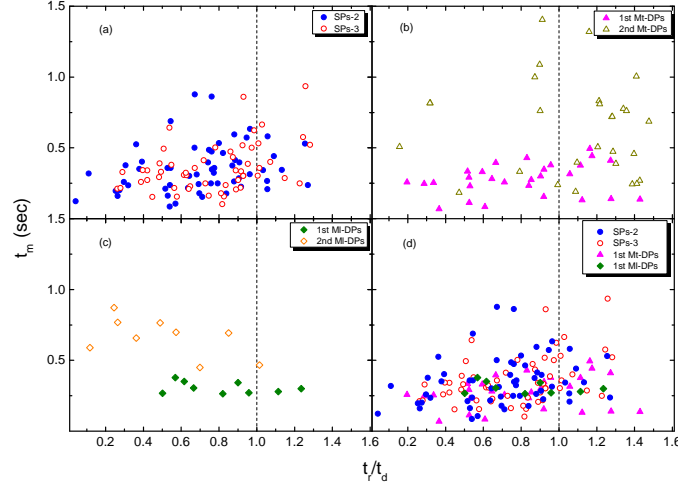


**Figure 6.** Correlations between the  $t_m$  and the  $t_r/t_d$  of all three kinds of sGRB pulses. The symbols are the same as Figure 2.

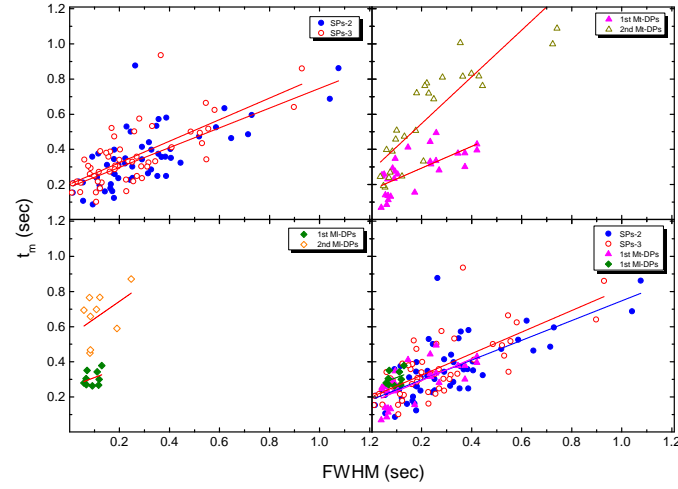


**Figure 7.** Correlations between the  $t_m$  and the FWHM of all three kinds of sGRB pulses. The symbols are as same as Figure 2. The lines are the best fits.

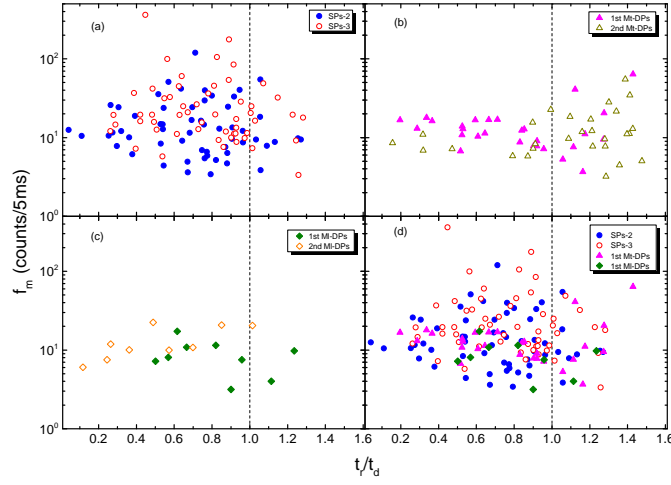


**Figure 8.** Correlations between the pulse amplitude  $f_m$  and the  $t_r/t_d$  of all three kinds of sGRB pulses. The symbols are the same as Figure 2.

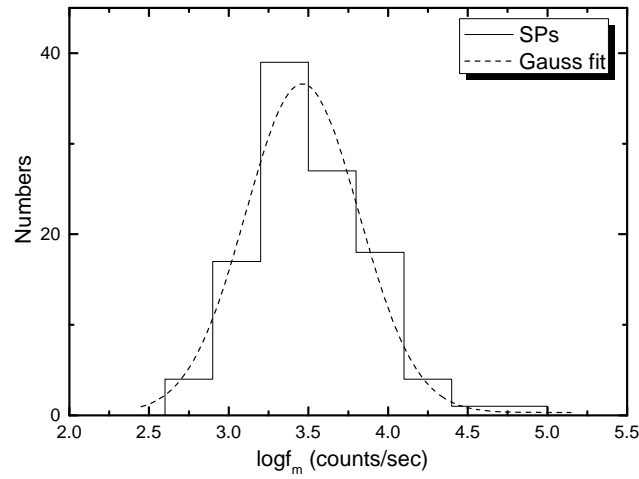


**Figure 9.** Distribution of the  $f_m$  of the 111 SPs. The dash line represents the best fit with a log-normal function.



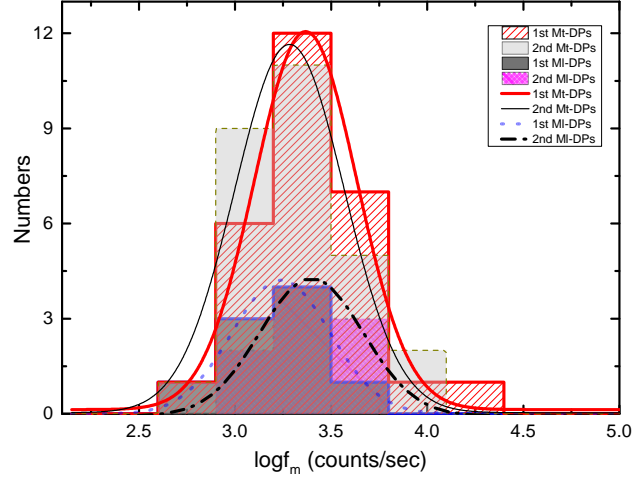


**Figure 10.** Distributions of the  $\log f_m$  for the 9 MI-DPs and the 28 Mt-DPs. On the upper region, the light gray and hatched areas correspondingly represent the distributions of the 1st and the 2nd pulses of the Mt-DPs; On the lower region, the dark gray and dense hatched areas represent the distributions of the 1st and the 2nd pulses of the MI-DPs, respectively. The solid and dash lines are the best fits with a log-normal function to the distributions.

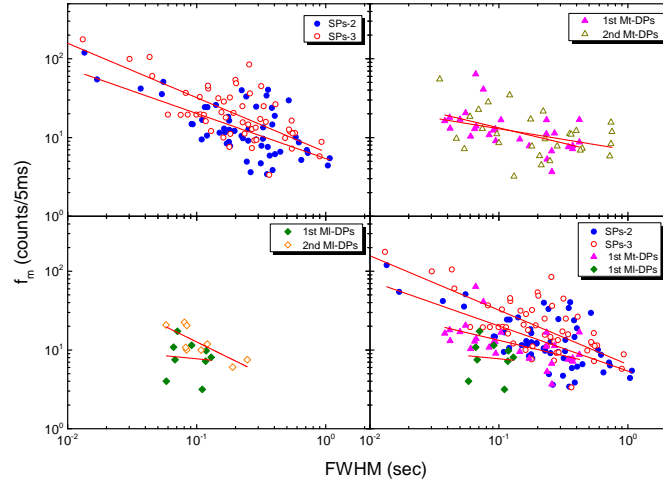


**Figure 11.** Correlations between the  $f_m$  and the FWHM of all three kinds of sGRB pulses. The symbols are the same as Figure 2.

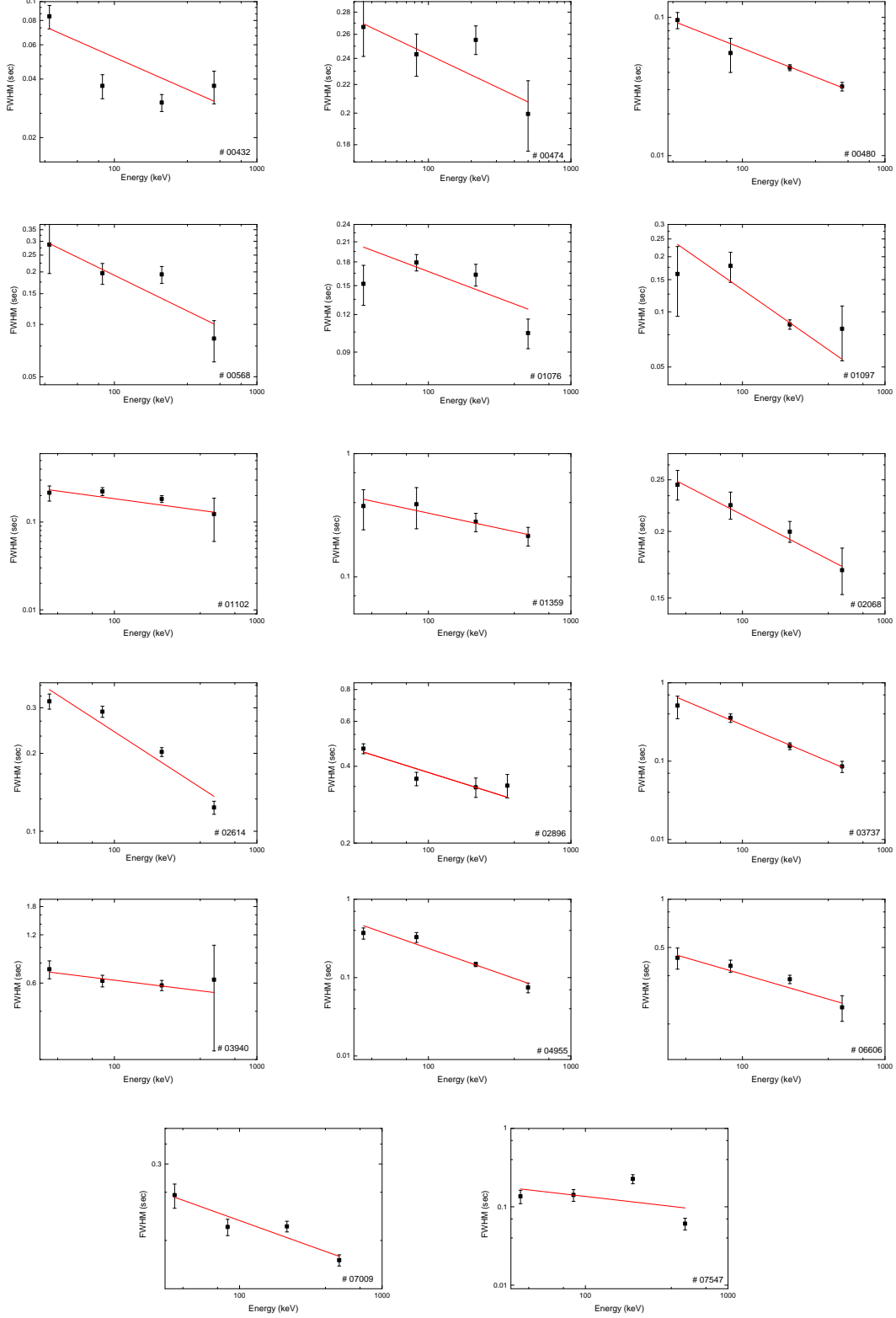


**Figure 12.** Examples of the dependence of the FWHM on the photon energy with a power law anti-correlation for the SPs. Note that the inferred errors of the FWHM for the pulses in Ch4 of # 02068 and in Ch3 of # 00432 are so large that we just assume a 10% of the FWHM as an error estimation in our calculations, as reported in [Norris et al. \(1996\)](#) and [Norris et al. \(2005\)](#).

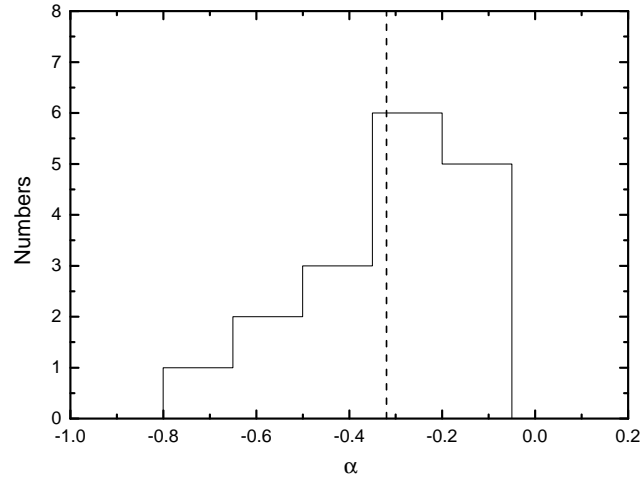


**Figure 13.** Distribution of the  $\alpha$  in the  $FWHM \propto E^\alpha$  relation for 17 SPs with negative power law indexes. The vertical dash line indicates the mean value of  $\alpha \simeq -0.32$ .

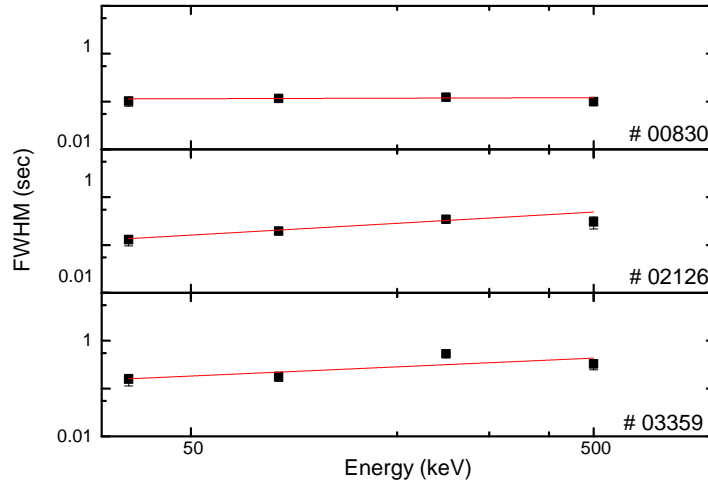


**Figure 14.** Examples of the dependence of the FWHM on the photon energy with a positive power-law correlation for the three SPs numbered with #00830, #02126 and #03359.

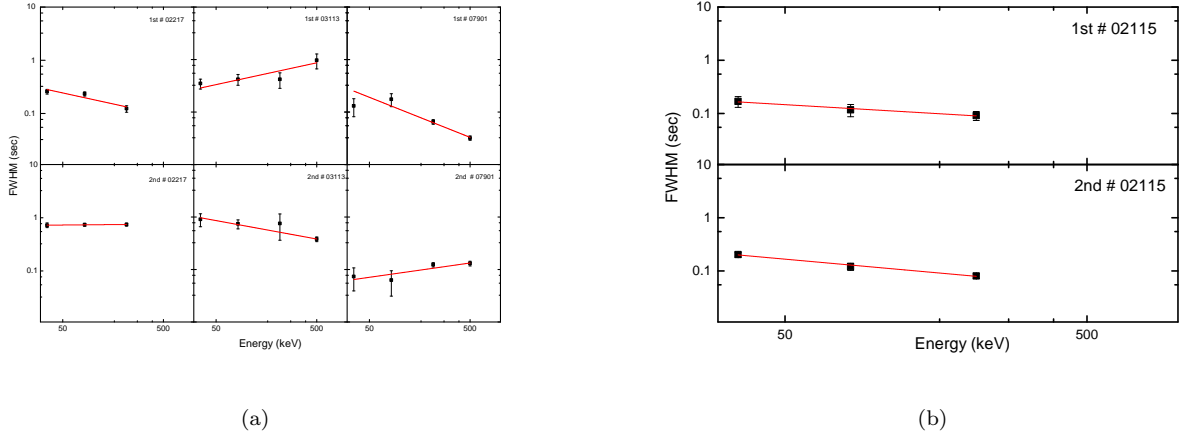


**Figure 15.** (a) The dependencies of the FWHM on the photon energy for the Mt-DP sGRBs. Note that the inferred errors of the FWHM for the 1st and the 2nd pulses in Ch2 of # 02217, Ch1 and Ch3 of # 07901 and the 2nd pulse in Ch4 of # 03113 are so large that we just take a 10% of the FWHM as an error estimation in our calculations. (b) The dependencies of the width on the photon energy for the first (top panel) and the second (bottom panel) pulses of the Mt-DP sGRB (# 02115). Note that the inferred errors the FWHM in the second pulse are too large hence we instead take 10% of the widths as the estimated errors at each point, as reported in [Norris et al. \(1996\)](#) and [Norris et al. \(2005\)](#).

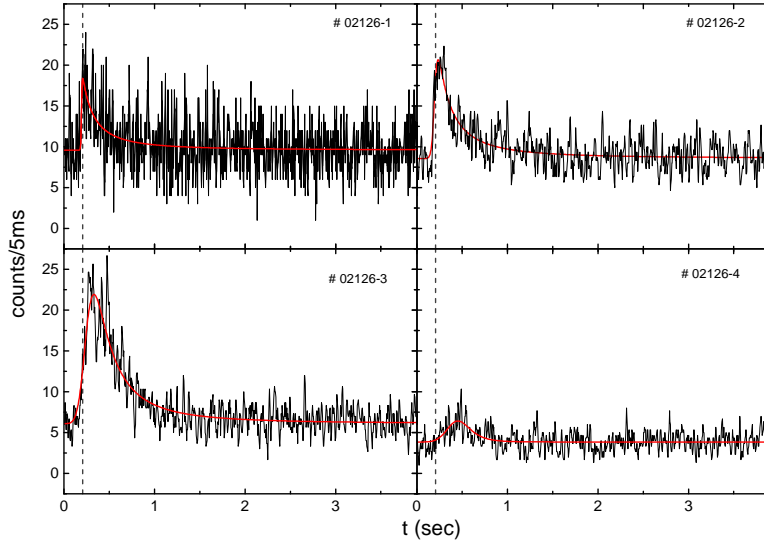


**Figure 16.** The pulse shape revolutions of the trigger # 02126 through Ch1 (upper left panel) , Ch2 (upper right panel) , Ch3 (lower left panel) and Ch4 (lower right panel). The peak time of pulse in Ch1 is marked by the vertical black dash line. Note that the dependence of the FWHM on the photon energy has a positive power-law index of  $\alpha = 0.48 \pm 0.13$ .



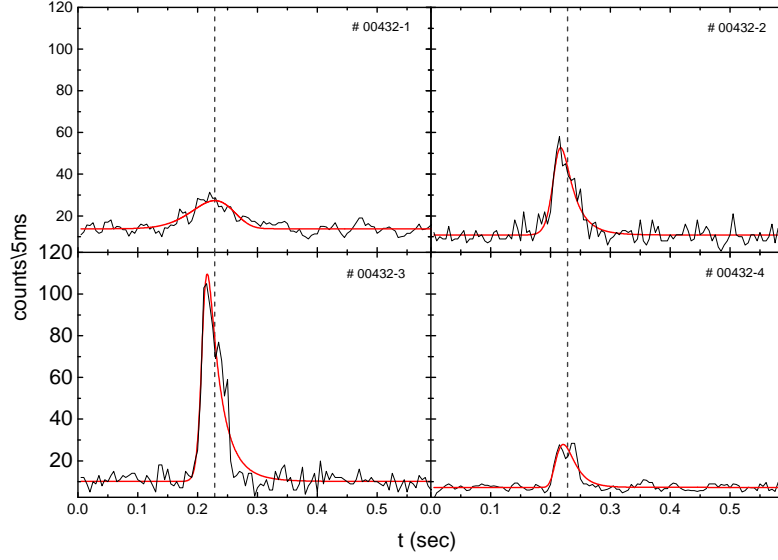


**Figure 17.** The pulse shape revolutions for the trigger # 00432 through Ch1 (upper left panel), Ch2 (upper right panel), Ch3 (lower left panel) and Ch4 (lower right panel). The peak time of pulse in Ch1 is marked by the vertical black dash line. Note that the dependence of the FWHM on the photon energy has a negative power-law index of  $\alpha = -0.32 \pm 0.15$ .

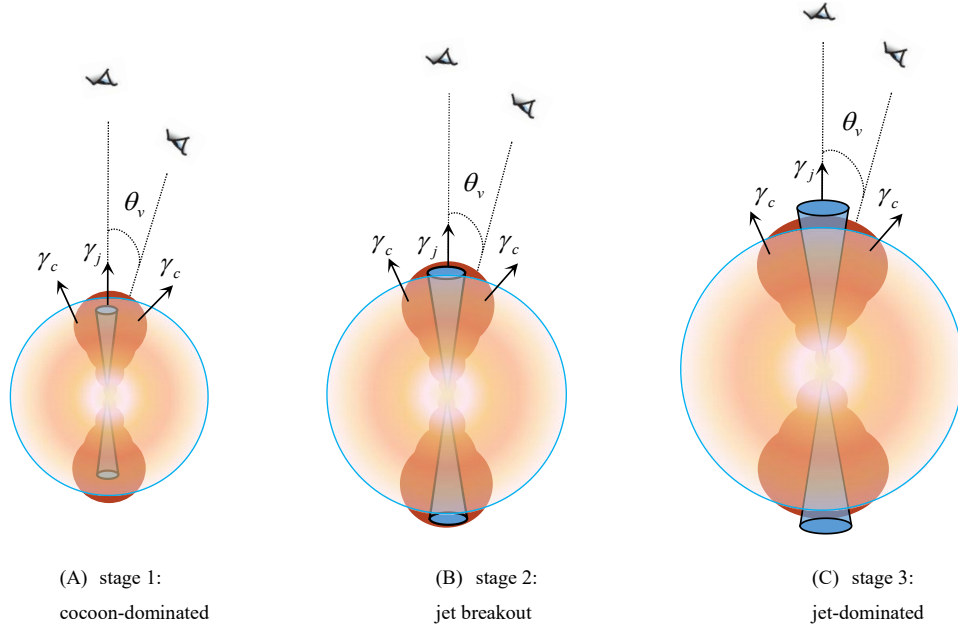


**Figure 18.** Schematic diagrams showing the geometry and evolution of a relativistically dynamical jet surrounded by a subrelativistic cocoon in some sGRBs at different prompt  $\gamma$ -ray phases. It has been assumed that the following three scenarios will continuously occur, in detail, the stage 1 is dominated by the cocoon, the stage 2 corresponds to the jet breakout, and the relativistic jet will be dominant in the stage 3.

**Table 1.** The best-fit parameters of the power-law correlation between the  $t_r$  and the  $t_d$ .

| <i>GRB</i>          | <i>Class</i> | $\chi^2_\nu$ | <i>Pearson's r</i> | <i>R</i> | $\beta$         |
|---------------------|--------------|--------------|--------------------|----------|-----------------|
| SPs                 | Ch2          | 3.64         | 0.80               | 0.64     | $0.89 \pm 0.09$ |
| SPs                 | Ch3          | 1.54         | 0.92               | 0.85     | $1.04 \pm 0.06$ |
| Mt-DPs <sup>†</sup> | Ch2/3        | 1.20         | 0.86               | 0.73     | $1.10 \pm 0.13$ |
| Mt-DPs <sup>‡</sup> | Ch2/3        | 1.39         | 0.84               | 0.69     | $0.83 \pm 0.11$ |
| MI-DPs <sup>†</sup> | Ch2/3        | 0.10         | 0.57               | 0.23     | $0.49 \pm 0.27$ |
| MI-DPs <sup>‡</sup> | Ch2/3        | 0.14         | 0.02               | -0.14    | $0.01 \pm 0.19$ |

**Table 2.** Asymmetric properties of different sGRBs.

| <i>GRB</i> | <i>Number</i> | <i>Maximum</i> | <i>mean(Median)</i> | <i>Minimum</i> |
|------------|---------------|----------------|---------------------|----------------|
| SPs        | Ch2+3         | 1.28           | 0.73(0.76)          | 0.04           |
| Mt-DPs     | 1st           | 1.23           | 0.82(0.82)          | 0.50           |
|            | 2nd           | 1.01           | 0.51(0.49)          | 0.12           |
| MI-DPs     | 1st           | 1.43           | 0.80(0.84)          | 0.20           |
|            | 2nd           | 1.48           | 1.07(1.21)          | 0.16           |
| Total      | -             | 1.48           | 0.79(0.81)          | 0.04           |
| TPs        | 1st           | -              | 1.06                | -              |
| (# 06715)  | 2nd           | -              | 0.57                | -              |
|            | 3th           | -              | 1.39                | -              |
| TPs        | 1st           | -              | 0.56                | -              |
| (# 07102)  | 2nd           | -              | 0.54                | -              |
|            | 3th           | -              | 0.93                | -              |

**Table 3.** The best-fit parameters of the correlation of the  $t_m$  with the FWHM.

| <i>GRB</i> | <i>Class</i> | $\chi^2_\nu$ | <i>Pearson's r</i> | <i>R</i> | $\mu$           |
|------------|--------------|--------------|--------------------|----------|-----------------|
| SPs        | Ch2          | 0.78         | 0.73               | 0.52     | $0.56 \pm 0.07$ |
| SPs        | Ch3          | 0.75         | 0.72               | 0.51     | $0.61 \pm 0.08$ |
| DPs        | Mt-DPs 1st   | 0.19         | 0.69               | 0.45     | $0.62 \pm 0.13$ |
|            | Mt-DPs 2nd   | 0.55         | 0.91               | 0.81     | $1.33 \pm 0.12$ |
| DPs        | MI-DPs 1st   | 0.01         | 0.35               | 0.00     | $0.54 \pm 0.54$ |
|            | MI-DPs 2nd   | 0.13         | 0.44               | 0.08     | $0.99 \pm 0.77$ |

**Table 4.** The best-fit parameters of the correlation of the  $f_m$  with the FWHM.

| <i>GRB</i> | <i>Class</i> | $\chi^2_\nu$ | <i>Pearson's r</i> | <i>R</i> | $\nu$            |
|------------|--------------|--------------|--------------------|----------|------------------|
| SPs        | Ch2          | 3.63         | -0.64              | 0.40     | $-0.57 \pm 0.09$ |
| SPs        | Ch3          | 3.52         | -0.73              | 0.53     | $-0.69 \pm 0.09$ |
| DPs        | Mt-DPs 1st   | 1.18         | -0.54              | 0.27     | $-0.39 \pm 0.12$ |
|            | Mt-DPs 2nd   | 1.80         | -0.38              | 0.11     | $-0.27 \pm 0.13$ |
| DPs        | MI-DPs 1st   | 0.41         | -0.09              | -0.13    | $-0.16 \pm 0.65$ |
|            | MI-DPs 2nd   | 0.12         | -0.79              | 0.58     | $-0.80 \pm 0.23$ |

**Table 5.** The best-fit parameters of the correlation between the FWHM and the average energy of photons in each channel.

| <i>GRB</i> | <i>Trigger number</i> | <i>Class</i> | $\alpha$         | $\chi^2_\nu$ | <i>Pearson's r</i> | <i>R</i> |
|------------|-----------------------|--------------|------------------|--------------|--------------------|----------|
| SPs        | 00432                 | negative     | $-0.32 \pm 0.15$ | 12.50        | -0.83              | 0.53     |
| SPs        | 00474                 | negative     | $-0.10 \pm 0.04$ | 3.09         | -0.89              | 0.69     |
| SPs        | 00480                 | negative     | $-0.41 \pm 0.03$ | 0.29         | -1.00              | 0.99     |
| SPs        | 00568                 | negative     | $-0.40 \pm 0.10$ | 3.35         | -0.94              | 0.84     |
| SPs        | 01076                 | negative     | $-0.18 \pm 0.12$ | 2.00         | -0.74              | 0.32     |
| SPs        | 01097                 | negative     | $-0.54 \pm 0.18$ | 1.57         | -0.90              | 0.72     |
| SPs        | 01102                 | negative     | $-0.22 \pm 0.06$ | 2.39         | -0.94              | 0.81     |
| SPs        | 01359                 | negative     | $-0.25 \pm 0.05$ | 0.15         | -0.96              | 0.89     |
| SPs        | 02068                 | negative     | $-0.14 \pm 0.01$ | 0.5          | -0.83              | 0.53     |
| SPs        | 02614                 | negative     | $-0.36 \pm 0.07$ | 7.82         | -0.96              | 0.89     |
| SPs        | 02896                 | negative     | $-0.18 \pm 0.09$ | 1.91         | -0.89              | 0.58     |
| SPs        | 03737                 | negative     | $-0.77 \pm 0.06$ | 0.51         | -0.99              | 0.98     |
| SPs        | 03940                 | negative     | $-0.11 \pm 0.03$ | 0.16         | -0.94              | 0.82     |
| SPs        | 04955                 | negative     | $-0.64 \pm 0.11$ | 1.30         | -0.97              | 0.91     |
| SPs        | 06606                 | negative     | $-0.26 \pm 0.04$ | 2.34         | -0.97              | 0.92     |
| SPs        | 07009                 | negative     | $-0.32 \pm 0.08$ | 3.14         | -0.95              | 0.84     |
| SPs        | 07547                 | negative     | $-0.21 \pm 0.30$ | 13.53        | -0.44              | -0.20    |
| SPs        | 00830                 | positive     | $0.02 \pm 0.07$  | 0.91         | 0.21               | -0.43    |
| SPs        | 02126                 | positive     | $0.48 \pm 0.13$  | 2.66         | 0.93               | 0.80     |
| SPs        | 03359                 | positive     | $0.38 \pm 0.22$  | 19.36        | 0.77               | 0.38     |
| Mt-DPs     | 02217 1st             | negative     | $-0.41 \pm 0.16$ | 4.29         | -0.93              | 0.74     |
| Mt-DPs     | 02217 2nd             | positive     | $0.02 \pm 0.01$  | 0.02         | 0.95               | 0.79     |
| Mt-DPs     | 03113 1st             | positive     | $0.42 \pm 0.15$  | 1.35         | 0.89               | 0.68     |
| Mt-DPs     | 03113 2nd             | negative     | $-0.35 \pm 0.04$ | 0.24         | -0.99              | 0.96     |
| Mt-DPs     | 07901 1st             | negative     | $-0.72 \pm 0.40$ | 3.60         | -0.79              | 0.43     |

*Table 5 continued*

**Table 5** (*continued*)

| <i>GRB</i> | <i>Trigger number</i> | <i>Class</i> | $\alpha$         | $\chi^2_\nu$ | <i>Pearson's r</i> | <i>R</i> |
|------------|-----------------------|--------------|------------------|--------------|--------------------|----------|
| Mt-DPs     | 07901 2nd             | positive     | $0.12 \pm 0.01$  | 1.31         | 0.99               | 0.96     |
| Ml-DPs     | 02115 1st             | negative     | $-0.33 \pm 0.04$ | 1.50         | -0.99              | 0.97     |
| Ml-DPs     | 02115 2nd             | negative     | $-0.51 \pm 0.03$ | 0.11         | -1.00              | 0.99     |



## REFERENCES

- Beniamini, P., & Nakar, E. 2019, *MNRAS*, 482, 5430
- Bostanci, Z. F., Kaneko, Y., & Göğüş, E. 2013, *MNRAS*, 428, 1623
- Campana, S., Mangano, V., Blustin, A. J., et al. 2006, *Nature*, 442, 1008
- Fenimore, E. E., in't Zand, J. J. M., Norris, J. P., et al. 1995, *ApJL*, 448, L101
- Ghirlanda, G., Salafia, O. S., Paragi, Z., et al. 2019, *Science*, 363, 968
- Ghirlanda, G., Bernardini, M. G., Calderone, G., et al. 2015, *Journal of High Energy Astrophysics*, 7, 81
- Goldstein, A., Veres, P., Burns, E., et al. 2017, *ApJL*, 848, L14
- Golkhou, V. Z., Butler, N. R., & Littlejohns, O. M. 2015, *ApJ*, 811, 93
- Hakkila, J., Giblin, T. W., Norris, J. P., Fragile, P. C., & Bonnell, J. T. 2008, *ApJL*, 677, L81
- Hakkila, J., & Preece, R. D. 2011, *ApJ*, 740, 104
- Hakkila, J., & Preece, R. D. 2014, *ApJ*, 783, 88
- Hakkila, J., Lien, A., Sakamoto, T., et al. 2015, *ApJ*, 815, 134
- Hakkila, J., Horváth, I., Hofesmann, E., et al. 2018a, *ApJ*, 855, 101
- Hakkila, J., Lesage, S., McAfee, S., et al. 2018b, *ApJ*, 863, 77
- Hu, Y. D., Liang, E. W., Xi, S. D., et al. 2014, *ApJ*, 789, 145
- Klebesadel, R. W., Strong, I. B., & Olson, R. A. 1973, *ApJL*, 182, L85
- Kocevski, D., Ryde, F., & Liang, E. 2003, *ApJ*, 596, 389
- Kouveliotou, C. 1994, *ApJS*, 92, 637
- Lan, L., Lü, H.-J., Zhong, S.-Q., et al. 2018, *ApJ*, 862, 155
- Li, L. 2019, *ApJS*, 242, 16
- Li, X. J., Zhang, Z. B., Zhang, K., et al. 2020, *ApJ*, in preparation
- Lyutikov, M., & Usov, V. V. 2000, *ApJL*, 543, L129
- Lin, D.-B., Mu, H.-J., Lu, R.-J., et al. 2017, *ApJ*, 840, 95
- Lien, A., Sakamoto, T., Barthelmy, S. D., et al. 2016, *ApJ*, 829, 7
- Liang, E.-W., Zhang, B.-B., & Zhang, B. 2007, *ApJ*, 670, 565
- Mooley, K. P., Nakar, E., Hotokezaka, K., et al. 2018, *Nature*, 554, 207
- Mooley, K. P., Deller, A. T., Gottlieb, O., et al. 2018, *Nature*, 561, 355
- Margutti, R., Chincarini, G., Granot, J., et al. 2011, *MNRAS*, 417, 2144
- McBreen, S., Quilligan, F., McBreen, B., et al. 2001, *A&A*, 380, L31
- Norris, J. P., Nemiroff, R. J., Bonnell, J. T., et al. 1996, *ApJ*, 459, 393
- Norris, J. P., Bonnell, J. T., & Watanabe, K. 1999, *ApJ*, 518, 901
- Norris, J. P., Bonnell, J. T., Kazanas, D., et al. 2005, *ApJ*, 627, 324
- Norris, J. P., & Bonnell, J. T. 2006, *ApJ*, 643, 266
- Norris, J. P., Gehrels, N., & Scargle, J. D. 2011, *ApJ*, 735, 23
- Peng, Z.-Y., Qin, Y.-P., Zhang, B.-B., et al. 2006, *MNRAS*, 368, 1351
- Qin, Y.-P., Zhang, Z.-B., Zhang, F.-W., et al. 2004, *ApJ*, 617, 439
- Qin, Y.-P. 2002, *A&A*, 396, 705
- Quilligan, F., Hurley, K. J., McBreen, B., et al. 1999, *A&AS*, 138, 419
- Quilligan, F., McBreen, B., Hanlon, L., et al. 2002, *A&A*, 385, 377
- Rhoads, J. E. 1999, *ApJ*, 525, 737
- Ryde, F., & Svensson, R. 2000, *ApJL*, 529, L13
- Ryde, F., & Svensson, R. 2002, *ApJ*, 566, 210
- Sari, R. 1999, *ApJL*, 524, L43
- Spada, M., Panaitescu, A., & Mészáros, P. 2000, *ApJ*, 537, 824
- Shao, L., Zhang, B.-B., Wang, F.-R., et al. 2017, *ApJ*, 844, 126
- von Kienlin, A., Veres, P., Roberts, O. J., et al. 2019, *ApJ*, 876, 89
- Willingale, R., O'Brien, P. T., Osborne, J. P., et al. 2007, *ApJ*, 662, 1093
- Wu, Y., & MacFadyen, A. 2018, *ApJ*, 869, 55
- Zhang, F.-W. 2008, *ApJ*, 685, 1052
- Zhang, Z. B., Xie, G. Z., Deng, J. G., et al. 2006, *MNRAS*, 373, 729
- Zhang, Z. B., & Qin, Y. P. 2005, *MNRAS*, 363, 1290
- Zhong, S.-Q., Dai, Z.-G., Cheng, J.-G., et al. 2019, *ApJ*, 884, 25
- Zhang, Z. B., Xie, G. Z., Deng, J. G., et al. 2007, *Astronomische Nachrichten*, 328, 99
- Zhang, Z. B., & Xie, G. Z. 2007, *Ap&SS*, 310, 19
- Zhang, B.-B., Zhang, B., Castro-Tirado, A. J., et al. 2018, *Nature Astronomy*, 2, 69
- Zhang, Z.-B., Deng, J.-G., Lu, R.-J., et al. 2006, *ChJA&A*, 6, 312